

Tight Constraint Prediction of Six-Degree-of-Freedom Transformer-based Powered Descent Guidance

Julia Briden*

2101 E NASA Pky, Houston, TX, 77058 USA

Trey Gurga †

Department of Aeronautics and Astronautics, Massachusetts Institute of Technology, 77 Massachusetts Avenue, Cambridge, Massachusetts, 02139 USA

Breanna Johnson ‡

2101 E NASA Pky, Houston, TX, 77058 USA

Abhishek Cauligi §

NASA Jet Propulsion Laboratory, California Institute of Technology, 4800 Oak Grove Dr, Pasadena, CA 91109 USA

Richard Linares ¶

Department of Aeronautics and Astronautics, Massachusetts Institute of Technology, 77 Massachusetts Avenue, Cambridge, Massachusetts, 02139 USA

This work introduces Transformer-based Successive Convexification (T-SCvx), an extension of Transformer-based Powered Descent Guidance (T-PDG), generalizable for efficient six-degree-of-freedom (DoF) fuel-optimal powered descent trajectory generation. Our approach significantly enhances the sample efficiency and solution quality for nonconvex-powered descent guidance by employing a rotation invariant transformation of the sampled dataset. T-PDG was previously applied to the 3-DoF minimum fuel powered descent guidance problem, improving solution times by up to an order of magnitude compared to lossless convexification (LCvx). By learning to predict the set of tight or active constraints at the optimal control problem’s solution, Transformer-based Successive Convexification (T-SCvx) creates the minimal reduced-size problem initialized with only the tight constraints, then uses the solution of this reduced problem to warm-start the direct optimization solver. 6-DoF powered descent guidance is known to be challenging to solve quickly and reliably due to the nonlinear and non-convex nature of the problem, the discretization scheme heavily influencing solution validity, and reference trajectory initialization determining algorithm convergence or divergence. Our contributions in this work address these challenges by extending T-PDG to learn the set of tight constraints for the successive convexification (SCvx) formulation of the 6-DoF powered descent guidance problem. In addition to reducing the problem size, feasible and locally optimal reference trajectories are also learned to facilitate convergence from the initial guess. T-SCvx enables onboard computation of real-time guidance trajectories, demonstrated by a 6-DoF Mars powered landing application problem.

I. Nomenclature

Variables

*Advanced Mission Design and GN&C Engineer, Amentum, NASA Johnson Space Center, 2101 E NASA Pky, Houston, TX 77058 USA, and AIAA Member.

†Undergraduate Student, Department of Aeronautics and Astronautics, 77 Massachusetts Avenue, Cambridge, Massachusetts, 02139 USA, and AIAA Student Member.

‡Aerospace Engineer, Flight Mechanics and Trajectory Design Branch, EG5, NASA Johnson Space Center, 2101 E NASA Pky, Houston, TX, Senior Member AIAA.

§Robotics Technologist, Jet Propulsion Laboratory, California Institute of Technology, Pasadena, CA 91109, USA.

¶Rockwell International Career Development Professor and Associate Professor, Department of Aeronautics and Astronautics, 125 Massachusetts Avenue. Senior Member AIAA.

$\alpha_{\dot{m}}$	=	fuel consumption rate
$\beta_{\dot{m}}$	=	vacuum specific impulse
δ_{\max}	=	maximum gimbal angle
ν	=	virtual control
$\mathbf{\Omega}_{\omega_{\mathcal{B}}(t)}$	=	quaternion transform
ω	=	penalty coefficients
$\omega_{\mathcal{B}}$	=	angular velocity
ϕ	=	pitch angle
σ^i	=	time-scaling factor
τ_i	=	set of tight constraints for sample i
θ_i	=	neural network input parameters for sample i
θ_{\max}	=	maximum pointing angle
A	=	state dynamics matrix
B	=	control dynamics matrix
C	=	future control dynamics matrix
$C_{I \leftarrow \mathcal{B}}$	=	transformation matrix
d_k	=	number of columns in the transformer weight matrix
\mathbf{e}	=	inertial frame unit vector (e_1, e_2, e_3), defined at the landing site, with e_1 pointing in the opposite direction of \mathbf{g}_I
\mathbf{g}_I	=	gravitational acceleration
H_γ	=	glideslope matrix
H_θ	=	pointing angle matrix
h_{gs}	=	glideslope constraint vector
$h = 1, \dots, H$	=	transformer head
I	=	identity
$\mathbf{J}_{\mathcal{B}}$	=	moment of inertia
K	=	final time step
K_h	=	transformer key matrices
k	=	iteration number
$M_{\mathcal{B}}$	=	net propulsive and aerodynamic torque acting on the vehicle equal to $r_{T,\mathcal{B}} \times T_{\mathcal{B}}(t) + r_{\text{cp},\mathcal{B}} \times A_{\mathcal{B}}(t)$ [N m]
m	=	mass
m_{wet}	=	wet mass
N	=	number of discretization nodes
O_h	=	transformer attention output
Q_h	=	transformer key matrices
P_{amb}	=	ambient atmospheric pressure [N/m ²]
q	=	spacecraft quaternion
\mathbf{r}_I	=	position
\mathbf{s}	=	state
s_i	=	neural network strategy output for sample i
t_f	=	final time
$\mathbf{T}_{\mathcal{B}}$	=	thrust
T_{\max}	=	maximum thrust
T_{\min}	=	minimum thrust
V_h	=	transformer value matrices
\mathbf{v}_I	=	velocity
z	=	optimization problem parameter

Functions

$f : \mathbb{R}^n \rightarrow \mathbb{R}$	=	cost function
$\mathbf{g} : \mathbb{R}^{n_x} \times \mathbb{R}^{n_u} \times \mathbb{R} \rightarrow \mathbb{R}^{n_c}$	=	vector of non-convex constraints
$\mathbf{h} : \mathbb{R}^{n_x} \times \mathbb{R}^{n_u} \times \mathbb{R} \rightarrow \mathbb{R}^{n_b}$	=	vector of convex constraints

Notation

\otimes	=	quaternion multiplication
Ω	=	skew-symmetric matrix defined such that the quaternion kinematics hold [1]
\hat{e}	=	unit direction vector
θ	=	parametric problem parameters
\mathcal{B}	=	problem parameters in the body-fixed reference frame
\mathcal{I}_{eq}	=	set of non-convex equality constraints
$\mathcal{I}_{\text{ineq}}$	=	set of non-convex inequality constraints
$\mathcal{J}_{\text{ineq}}$	=	set of convex inequality constraints
\mathcal{I}	=	problem parameters in the inertial reference frame
$q_{\mathcal{B} \leftarrow \mathcal{I}}^*$	=	conjugate of $q_{\mathcal{B} \leftarrow \mathcal{I}}$
q_{id}	=	identity quaternion

II. Introduction

INCREASINGLY complex and high mass planetary missions require autonomous long-horizon trajectory generation to achieve dynamically feasible Powered Descent Guidance (PDG). Moreover, there is a pressing need to generate fuel-optimal trajectories in order to satisfy the mass and safety margin requirements necessary for enabling human-rated vehicles. A key challenge in applying existing methods is that the radiation-hardened processors used in most aerospace applications struggle to satisfy the sub-second trajectory generation requirements necessary to enable onboard usage. While current work in custom solver implementations for 6-degree-of-freedom (DoF) PDG has achieved sub-millisecond level runtimes, these only hold for short horizon problems of less than 50 discretization nodes [2]. Recently, data-driven methods have emerged as a promising tool in reducing onboard computation times for numerous classes of algorithms [3, 4] and researchers have introduced methods such as Transformer-based Powered Descent Guidance (T-PDG) to bridge this gap in long-horizon trajectory generation [5]. This method utilizes previous runs of the 3-DoF Lossless Convexification (LCvx) implementation of the Mars-powered descent landing problem to train a non-linear mapping between problem parameters and the set of tight constraints that defines the optimal problem solution. The reduced problem, defined by equality and identified tight constraints, is then solved and used as an initial guess for the full problem to ensure feasibility and constraint satisfaction. This work extends T-PDG to 6-DoF, introducing Transformer-based Successive Convexification (T-SCvx), on a smaller rotation-invariant training and test set of trajectories generated using Successive Convexification (SCvx). Additionally, variable-horizon outputs, which include a trajectory and control guess, are predicted to facilitate fast and reliable convergence to a locally optimal solution.

By enabling the deployment of autonomous optimal guidance technologies for spacecraft powered descent landing trajectory generation, a wider range of dispersions and uncertainties can be recovered, improving the mission safety margins and enabling the exploration of increasingly challenging and scientifically rich landing sites.

Optimal solutions can be formulated either using indirect or direct methods. Indirect methods, including Universal Powered Guidance (UPG) and Propellant-Optimal PDG, solve for the necessary optimality conditions for the optimal control problem by solving a two-point boundary value problem corresponding to the state and costate dynamics and their boundary conditions [6, 7]. For common classes of problems, application of Pontryagin’s Maximum Principle [8] yield analytical solutions, but these methods fall short for trajectory generation as they are applicable to a limited set of mission constraints and objective functions [9–12]. Moreover, while both analytical and indirect methods are computationally efficient, significant simplifications of the dynamics and constraints are required for both problem formulations. As such, bang-bang control strategies and linear gravity assumptions are often required and both state and control inequality constraints are not easily implementable in a root-finding framework [6, 7].

In contrast, direct methods, often formulated as sequential convex programs (SCPs) [13–21] or sequential quadratic programs (SQPs) [22–29], compute locally optimal solutions for a general class of non-convex constrained optimization problems. A special case of direct methods is the second-order cone program (SOCP), which results from the lossless convexification of nonconvex cost, dynamics, and control constraints, often applied to the 3-DoF powered descent guidance problem [30–39]. In this case, the nonconvex problem formulation can be formulated as a convex SOCP, enabling the recovery of the globally optimal solution, including certificates of convergence and infeasibility via an interior point method (IPM) algorithm [40, 41]. An extension of this work based on dual-quaternions allowed for 6-DoF motion, but required piecewise-affine approximations of the nonlinear dynamics, degrading solution accuracy as the temporal resolution of the discretization decreases [42, 43]. This special case of problems also relies on a line search to recover the optimal final time due to the non-convexities introduced by allowing a free final time [21].

To generalize beyond the narrow class of problems that can be losslessly convexified, SCvx can solve the general class of non-convex optimal control problems while forgoing the rigorous optimality and convergence guarantees provided by convex solvers [40]. SCvx transforms the non-convex full problem into a sequence of convex subproblems, which can be solved successfully until convergence [17–19, 19, 20]. SCP-based methods have been generalized beyond powered descent guidance to non-convex control-affine systems and incorporated indirect optimal control methods for accelerated convergence, as well as for mixed-integer convex programs (MICPs) [44–46]. In this work, we focus on efficiently solving the free-final-time 6-DoF SCvx problem formulation by predicting the reduced problem defined by only the tight constraints and a dynamically feasible initial guess via a transformer-based deep neural network. Full constraint satisfaction is guaranteed by warm-starting the full problem with the reduced problem’s solution.

This work aims to improve the computational efficiency of the 6-DoF powered descent guidance problem with free ignition time, including aerodynamic forces and conditional enforced constraints [2]. While this problem setup enables high-fidelity locally fuel-optimal trajectory generation via explicit inclusion of operational and mission constraints, directly solving the problem in real-time is challenging due to nonlinear dynamics and non-convex state and control constraints, which do not yield close-form solutions. Furthermore, the convergence of this nonconvex problem depends heavily on both the discretization scheme and the development of a suitable initial guess trajectory to initialize the solver. This work focuses on efficiently solving the free-final-time 6-DoF SCvx problem formulation by predicting the reduced problem defined by only the tight constraints and a dynamically feasible initial guess via a transformer-based deep neural network. Full constraint satisfaction is guaranteed by warm-starting the full problem with the reduced problem’s solution.

A. Contributions

This work develops a 6-DoF T-SCvx with Mars landing, benchmarks against SCvx algorithms, and lookup table-based methods. T-SCvx significantly improves the convergence and computational efficiency of successive convexification by 1) enabling efficient sub-problem generation and warm-starting using Transformer-based tight constraint prediction, 2) utilizing rotation-invariant data augmentation, lowering the number of optimization problem samples required for training to under 2,000 samples, and 3) ensuring feasibility by only warm starting the convex subproblems, computing and solving with the penalty cost for the full problem. Figure 2 shows the T-SCvx inputs, θ_i , and strategy, s_i , for a given test case, i .

B. Outline

This paper is formulated as follows. Section III defines the 6-DoF minimum-fuel powered descent guidance problem formulation, details the Successive Convexification Sequential Convex Programming solver, defines tight constraint prediction and the recovered optima achieved using T-PDG, details the learning process, and defines the real-time test problem setup of T-SCvx for 6-DoF powered descent guidance. The T-SCvx results and analysis are in Section IV. Finally, areas of future work are described in Section V, and conclusions are stated in Section VI.

III. Methods

This section defines the generalized non-convex optimization problem and the associated notation, introduces the 6-DoF powered descent guidance problem and its SCvx formulation, formalizes the process of tight constraint prediction to construct a reduced problem, and defines the T-PDG algorithm, details the learning process, and finally covers the process of achieving real-time 6-DoF powered descent guidance with T-PDG using a Mars landing test case.

A. Non-Convex Optimization

The general non-convex continuous-time optimal control problem can be solved using a direct method by discretizing and then iteratively solving a system of equations, seeking to minimize cost while maintaining constraint satisfaction. The general discretized non-convex optimization problem can be written as:

Non-Convex Problem:

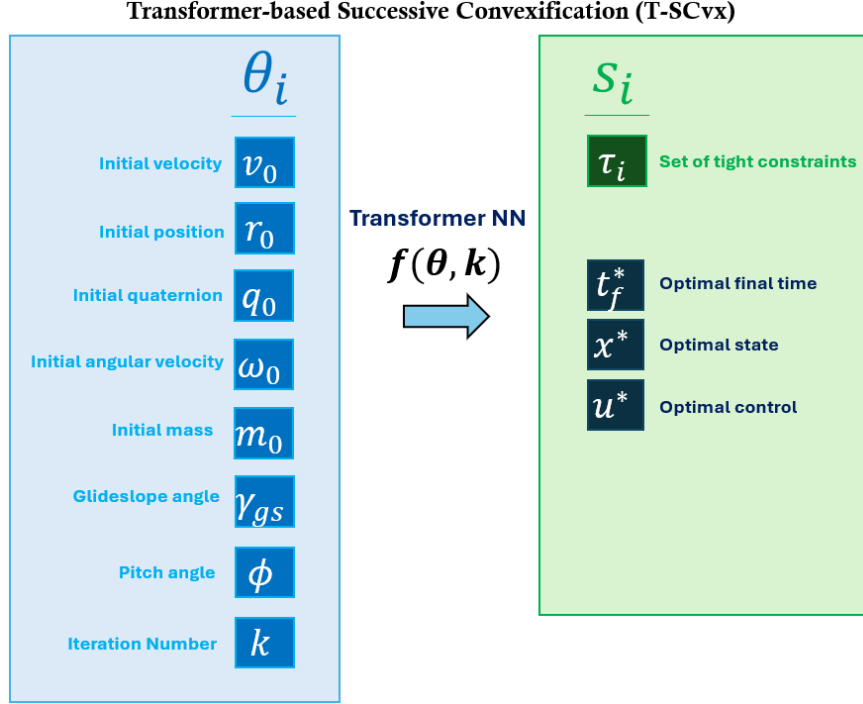


Fig. 1 T-SCvx inputs include the initial state and iteration number. The output of the constraint neural network, $\tau(\theta^{(i)})$, is the set of tight constraints, and the outputs of the initial guess neural network, $t_f^*(\theta^{(i)})$, $x_*(\theta^{(i)})$, and $u^*(\theta^{(i)})$, are the optimal final time, state, and control.

$$\begin{aligned}
 & \min_z f(z), \\
 & \text{subject to:} \\
 & g_i(z) = 0, \quad \forall i \in \mathcal{I}_{\text{eq}}, \\
 & g_i(z) \leq 0, \quad \forall i \in \mathcal{I}_{\text{ineq}}, \\
 & h_j(z) \leq 0, \quad \forall j \in \mathcal{J}_{\text{ineq}},
 \end{aligned} \tag{1}$$

where (1) describes the nonlinear system dynamics, the non-convex state and control constraints, and the convex state and control constraints. $\mathcal{I}_{\text{eq}} := \{1, 2, \dots, e\}$ represents the set of non-convex equality constraint indices, $\mathcal{I}_{\text{ineq}} := \{e + 1, \dots, p\}$ represents the set of non-convex inequality constraint indices, and $\mathcal{J}_{\text{ineq}} := \{1, 2, \dots, q\}$ represents the set of convex inequality indices. We assume that $g_i(z)$ and $h_j(z)$ are continuously differentiable for all $i \in \mathcal{I}_{\text{eq}} \cup \mathcal{I}_{\text{ineq}}$ and $j \in \mathcal{J}_{\text{ineq}}$. We further assume that $f(z) \in C^1$, but note that $f(z)$ can be an element of C^0 in practice.

B. Problem Formulation: Six-Degree-of-Freedom Powered Descent Guidance

This work aims to improve the computational efficiency of the 6-DoF powered descent guidance problem with free ignition time, including aerodynamic forces and conditional enforced constraints [2]. While this problem setup enables high-fidelity locally fuel-optimal trajectory generation via explicit inclusion of operational and mission constraints, directly solving the problem in real-time is challenging due to nonlinear dynamics and non-convex state and control constraints, which do not yield close-form solutions. Furthermore, the convergence of this nonconvex problem depends heavily on both the discretization scheme and the development of a suitable initial guess trajectory to initialize the solver.

The 6-DoF powered descent guidance problem formulation used in this work assumes that speeds are sufficiently low such that planetary rotation and changes in the planet's gravitational field are negligible. The spacecraft is assumed to be a rigid body with a constant center of mass and inertia and a fixed center of pressure. The propulsion consists of a single rocket engine that can be gimballed symmetrically about two axes bounded by a maximum gimbal angle δ_{max} . The engine is assumed to be throttleable between T_{min} and T_{max} , remaining on until the terminal boundary conditions

are met. An atmospheric drag model is included, assuming ambient atmospheric density and constant pressure. The minimum-fuel 6-DoF powered descent guidance problem is formulated as follows:

Cost Function:

$$\min_{t_f, \mathbf{T}_{\mathcal{B}}(t)} -m(t_f) \quad (2)$$

Boundary Conditions:

$$t_f \in [0, t_{f, \max}] \quad (3a)$$

$$m(t_0) = m_0 \quad (3b)$$

$$\mathbf{r}_I(t_0) = r_0 \quad (3c)$$

$$\mathbf{v}_I(t_0) = v_0 \quad (3d)$$

$$\omega_{\mathcal{B}}(t_0) = \omega_0 \quad (3e)$$

$$\mathbf{r}_I(t_f) = r_f \quad (3f)$$

$$\mathbf{v}_I(t_f) = v_f \quad (3g)$$

$$\mathbf{q}_{\mathcal{B} \leftarrow I}(t_f) = \mathbf{q}_f \quad (3h)$$

$$\omega_{\mathcal{B}}(t_f) = \omega_f \quad (3i)$$

Dynamics:

$$\dot{m}(t) = -\alpha_{\dot{m}} \|\mathbf{T}_{\mathcal{B}}(t)\|_2 - \beta_{\dot{m}} \quad (4a)$$

$$\dot{\mathbf{r}}_I(t) = \mathbf{v}_I(t) \quad (4b)$$

$$\dot{\mathbf{v}}_I(t) = \frac{1}{m(t)} \mathbf{C}_{I \leftarrow \mathcal{B}}(t) (\mathbf{T}_{\mathcal{B}}(t) + \mathbf{A}_{\mathcal{B}}(t)) + \mathbf{g}_I \quad (4c)$$

$$\dot{\mathbf{q}}_{\mathcal{B} \leftarrow I}(t) = \frac{1}{2} \Omega_{\omega_{\mathcal{B}}(t)} \mathbf{q}_{\mathcal{B} \leftarrow I}(t) \quad (4d)$$

$$\mathbf{J}_{\mathcal{B}} \dot{\omega}_{\mathcal{B}}(t) = \mathbf{r}_{T, \mathcal{B}} \times \mathbf{T}_{\mathcal{B}}(t) + \mathbf{r}_{cp, \mathcal{B}} \times \mathbf{A}_{\mathcal{B}}(t) - \omega_{\mathcal{B}}(t) \times \mathbf{J}_{\mathcal{B}} \omega_{\mathcal{B}}(t) \quad (4e)$$

State Constraints:

$$m_{\text{dry}} \leq m(t) \quad (5a)$$

$$\tan \gamma_{gs} \|H_{\gamma} \mathbf{r}_I(t)\|_2 \leq e_1 \cdot \mathbf{r}_I(t) \quad (5b)$$

$$\cos \theta_{\max} \leq 1 - 2 \|H_{\theta} \mathbf{q}_{\mathcal{B} \leftarrow I}(t)\|_2 \quad (5c)$$

$$\|\omega_{\mathcal{B}}(t)\|_2 \leq \omega_{\max} \quad (5d)$$

Control Constraints:

$$0 < T_{\min} \leq \|\mathbf{T}_{\mathcal{B}}(t)\|_2 \leq T_{\max} \quad (6a)$$

$$\cos \delta_{\max} \|\mathbf{T}_{\mathcal{B}}(t)\|_2 \leq e_3 \cdot \mathbf{T}_{\mathcal{B}}(t), \quad (6b)$$

where the cost function in Eq. (2) minimizes the mass at the final time, and the boundary conditions in Eq. (3) constrain the final time range and the initial and final states. The dynamics in Eq. (4) include mass depletion, translational state evolution, and rigid-body attitude dynamics. Finally, the state and control constraints in Equations (5) and (6) ensure that the mass is bounded, a glideslope constraint holds for landing, a maximum tilt angle is not exceeded, angular velocity is bounded, thrust is bounded, and the angle of attack is bounded. We refer the reader to [2, 47] for an extended discussion and derivation of the 6-DoF minimum fuel powered descent guidance problem

1. Successive Convexification

SCP solves non-convex direct optimization problems by iteratively solving a sequence of local convex approximations [21]. The SCP algorithm used in this work is SCvx due to its ability to solve non-convex constrained optimal control problems with global convergence and superlinear convergence-rate guarantees [19].

SCvx solves the desired optimal control problem to optimality by successively linearizing non-convex dynamics and constraints about the initial guess provided by the iteration prior, converting the nonconvex problem into a set of convex

subproblems. Furthermore, SCvx is guaranteed to recover local optimality if the converged solution is feasible with respect to the full problem and, if the Kurdyka-Lojasiewicz (KL) inequality holds at the converged solution, then the solution is unique [19].

At iteration k , SCvx uses a virtual control $v_i \in \mathbb{R}^{n_v}$ and $i \in 1 \dots N - 1$ and the trust region $r_k \in \mathbb{R}$ to facilitate convergence. At the $(k + 1)^{th}$ iteration a convex subproblem is defined as:

SCvx Convex Optimal Control Subproblem:

$$\begin{aligned} \min_{d,w} \quad & L^k(d, w) \\ \text{subject to:} \quad & u^k + w \in U, \\ & x^k + d \in X, \\ & \|w\| \leq r^k, \end{aligned} \tag{7}$$

where U and X are convex sets, often second-order cones, $L^k(d, w)$ is the penalized cost function, (x^k, u^k) are the current state and control iterates, $d_i := x_i - x_i^k$, and $w_i := u_i - u_i^k$. The iterates (x^k, u^k) are then successively updated using the linearized dynamics, which include virtual control and virtual buffer zones to mitigate artificial infeasibility:

$$v := [v_1^T, v_2^T, \dots, v_{N-1}^T]^T \in \mathbb{R}^{n_v(N-1)}, \tag{8}$$

$$s' := [s'_1{}^T, s'_2{}^T, \dots, s'_{N-1}{}^T]^T \in \mathbb{R}_+^{n_s(N-1)}. \tag{9}$$

The virtual control term v is left unconstrained, so any state in the feasible region of the convex subproblem is reachable in finite time, preventing artificial infeasibility after linearization. The virtual buffer zone $s'_i \in \mathbb{R}_+^{n_s}$ similarly maintains state reachability for the linearized non-convex state and control constraints. The first-order approximation of the dynamics and nonconvex constraints is then:

$$x_{i+1}^k + d_{i+1} = f(x_i^k, u_i^k) + A_i^k d_i + B_i^k w_i + E_i^k v_i, \tag{10}$$

$$s(x_i^k, u_i^k) + S_i^k d_i + Q_i^k w_i - s'_i \leq 0, \tag{11}$$

where $A_i^k := \frac{\partial}{\partial x_i} f(x_i, u_i)|_{x_i^k, u_i^k}$, $B_i^k := \frac{\partial}{\partial u_i} f(x_i, u_i)|_{x_i^k, u_i^k}$, $S_i^k := \frac{\partial}{\partial x_i} s(x_i, u_i)|_{x_i^k, u_i^k}$, $Q_i^k := \frac{\partial}{\partial u_i} s(x_i, u_i)|_{x_i^k, u_i^k}$, and $E_i^k \in \mathbb{R}^{n_x \times n_v}$ such that $\text{im}(E_i^k) = \mathbb{R}^{n_x}$. Algorithm 1 details the full SCvx algorithm.

Algorithm 1 The SCvx Algorithm

- 1: **procedure** SCvx($x^1, u^1, \lambda, \epsilon_{\text{tol}}$)
 2: **input:** Select initial state $x^1 \in X$ and control $u^1 \in U$. Initialize trust region radius $r^1 > 0$. Select penalty weight $\lambda > 0$, and parameters $0 < \rho_0 < \rho_1 < \rho_2 < 1$, $r_l > 0$ and $\alpha > 1, \beta > 1$.
 3: **while** not converged, i.e., $\Delta J^k > \epsilon_{\text{tol}}$ **do**
 4: **step 1:** At $(k + 1)$ -th succession, solve Equation 7 at (x^k, u^k, r^k) to get an optimal solution (d, w) .
 5: **step 2:** Compute the actual change in the penalty cost:

$$\Delta J^k = J(x^k, u^k) - J(x^k + d, u^k + w), \quad (12)$$

where $J(x, u) := C(x, u) + \sum_{i=1}^{N-1} \lambda_i P(x_{i+1} - f(x_i, u_i), s(x_i, u_i))$.

- 6: and the predicted change by the convex cost:

$$\Delta L^k = J(x^k, u^k) - L^k(d, w), \quad (13)$$

where $L^k(d, w) := C(x^k + d, u^k + w) + \sum_{i=1}^{N-1} \lambda_i P(E_i^k v_i, s'_i)$.

- 7: **if** $\Delta J^k = 0$ **then**
 8: stop, and return (x^k, u^k) ;
 9: **else**
 10: compute the ratio

$$\rho^k := \frac{\Delta J^k}{\Delta L^k}. \quad (14)$$

- 11: **end if**
 12: **step 3:**
 13: **if** $\rho^k < \rho_0$ **then**
 14: reject this step, contract the trust region radius, i.e., $r^k \leftarrow \frac{r^k}{\alpha}$ and go back to step 1;
 15: **else**
 16: accept this step, i.e., $x^{k+1} \leftarrow x^k + d$, $u^{k+1} \leftarrow u^k + w$, and update the trust region radius r^{k+1} by

$$r^{k+1} = \begin{cases} \frac{r^k}{\alpha}, & \text{if } \rho^k < \rho_1; \\ r^k, & \text{if } \rho_1 \leq \rho^k < \rho_2; \\ \beta r^k, & \text{if } \rho_2 \leq \rho^k. \end{cases} \quad (15)$$

- 17: **end if**
 18: $r^{k+1} \leftarrow \max\{r^{k+1}, r_l\}$, $k \leftarrow k + 1$, and go back to step 1.
 19: **end while**
 20: **return** (x^{k+1}, u^{k+1}) .
 21: **end procedure**
-

Following the guidance in [19], heuristic recommendations for parameter choice include choosing $\rho_0 \approx 0$, $\rho_1 \gtrsim 0$, $\rho_2 \lesssim 1$, $r_l \gtrsim 0$. Equation (21) compares the realized nonlinear cost reduction ΔJ^k to the predicted linear cost reduction ΔL^k using the previous, k^{th} , iteration. If the linear cost reduction over-predicts the realized nonlinear cost reduction, $\rho^k < \rho_0 \ll 1$, the step is rejected. Otherwise, the step is accepted, either contracting, maintaining, or growing the trust region size according to Eq. (22); shrinking the trust region when the linearization accuracy is acceptably deficient and growing when the linear cost reduction under-predicts or almost under-predicts the realized nonlinear cost reduction. Recent work has extended trust region updates to include state-dependent trust regions based on a nonlinearity index defined by the state transition matrix [48]. We note that a feasible initial guess is not required for SCvx and an infeasible initial guess does not affect the algorithm's convergence guarantees [19].

In this work, SCvx is applied to a discretized system, where the decision vector z is finite-dimensional and the exact penalty function used in Eq.(19) is defined as

$$J(z) := g_0(z) + \sum_{i \in \mathcal{I}_{\text{ncvx eq}}} \lambda_i |g_i(z)| + \sum_{i \in \mathcal{I}_{\text{ncvx ineq}}} \lambda_i \max(0, g_i(z)) + \sum_{i \in \mathcal{I}_{\text{cvx ineq}}} \tau_i \max(0, h_j(z)), \quad (16)$$

where the cost $g_0(z) \in C^1$, nonconvex equality and inequality constraints $g_i(z)$ and convex inequality constraints $h_i(z)$ are continuously differentiable for all $i \in \mathcal{I}_{\text{ncvx eq}} \cup \mathcal{I}_{\text{ncvx ineq}} \cup \mathcal{I}_{\text{cvx ineq}}$, and penalty weights $\lambda_i \geq 0$ and $\tau_i \geq 0$.

The only assumption required to achieve global weak convergence is the Linear Independence Constraint Qualification (LICQ): the columns of the matrices that make up the gradients of the active constraints are linearly independent at the local optimum [19]. If the LICQ is satisfied, Algorithm 1 always has limit points and any limit point \bar{z} is a stationary point of the non-convex penalty function, Equation (16). Furthermore, if \bar{z} is feasible for the original non-convex problem, then it is a Karush–Kuhn–Tucker (KKT) point of the problem.

To achieve strong convergence, where single limit point convergence is guaranteed, Lipschitz continuous gradients are required for the set of inequality constraints: $\exists L_i \geq 0$, such that $\|\nabla g_i(z_2) - \nabla g_i(z_1)\| \leq L_i \|z_2 - z_1\|$ for all $i = 0, \dots, p + q$, and the penalized cost function $J(z)$ must have the KL property [49]. If both these conditions hold, along with the LICQ, the sequence $\{z^k\}$ generated by SCvx always converges to a single limit point \bar{z} , and \bar{z} is a stationary point of the non-convex penalty $J(z)$. Additionally, if \bar{z} is feasible for the original non-convex problem, then it is a KKT point of that problem.

Finally, to maintain the superlinear convergence rate, strict complementary slackness must be met at the local optimum \bar{z} : $\lambda_i > 0$ for all active constraints and for $z^k \rightarrow \bar{z}$, there are at least $n_u(N - 1)$ binding constraints:

$$|\mathcal{A}_{\text{ncvx eq}}| + |\mathcal{A}_{\text{ncvx ineq}}| + |\mathcal{A}_{\text{cvx ineq}}| \geq n_u(N - 1), \quad (17)$$

where \mathcal{A} is the set of active, or tight, constraints. While bang-bang control solutions, which hold for the 3-DoF powered descent guidance problem, always uphold the binding assumption, the 6-DoF extension, which includes rotational dynamics and aerodynamics forces, is not guaranteed to yield this type of control solution. If both of these assumptions hold, along with the LICQ, superlinear convergence is theoretically guaranteed. Recent extensions of SCvx include penalty-based reformulations of path constraints, generalized time-dilation, multiple-shooting discretization, l_1 exact penalization of the nonconvex constraints, and the prox-linear method for convex-composite minimization [50]. For a full derivation and description of the SCvx algorithm and its convergence properties, see [19].

C. Tight Constraint Prediction

Consider the parametric formulation of the powered descent guidance problem, where the parameter vector $\theta \in \Theta \subseteq \mathbb{R}^{n_p}$ is drawn from a representative set of parameters and maps to a binary vector $\tau(\theta) \in \{0, 1\}^M$. Here, ones denote tight or active constraints at the indicated discretization nodes and zeros denote non-tight or inactive constraints. If the optimization problem is non-degenerate, then the tight constraints serve as the support constraints for the optimization problem, and removing any of the tight constraints would result in a decrease in the objective function for minimization problems [51]. T-PDG efficiently learns the mapping $\theta \rightarrow \tau(\theta)$ using prior runs of the constrained optimization problem to accurately predict the set of tight or active constraints at the globally (or locally) optimal solution.

For an inequality-constrained optimization problem (Equation (1)), the first order necessary conditions (i.e., KKT conditions), must hold.

Definition 1. *First Order Necessary Conditions: KKT Conditions*

$$\mathcal{L}(x, \lambda) = f(x) - \sum_{i \in \mathcal{I} \cup \mathcal{E}} \lambda_i c_i(x)$$

- 1) $\nabla_x \mathcal{L}(x^*, \lambda^*) = 0$
- 2) $c_i(x^*) = 0, \quad i \in \mathcal{E}$
- 3) $c_i(x^*) \geq 0, \quad i \in \mathcal{I}$
- 4) $\lambda_i^* \geq 0, \quad i \in \mathcal{I}$
- 5) $\lambda_i^* c_i(x^*) = 0, \quad i \in \mathcal{I} \cup \mathcal{E}$

The active \mathcal{A} set at any feasible x consists of the set of the equality constraint indices \mathcal{E}

Definition 2. *Active Set*

$$\mathcal{A}(x) = \mathcal{E} \cup \{i \in \mathcal{I} \mid c_i(x) = 0\}$$

Claim: When given the tight/active constraints set, the reduced problem defined by only the equality and active inequality constraints will recover the optimal solution for the original problem.

Proof. Assume there exists a feasible sequence $\{z_k\}$ such that $\nabla f(x^*)^T d < 0$. Then, for the limiting direction d :

$$\lim_{z_k \in s_d} \frac{z_k - x^*}{\|z_k - x^*\|} \rightarrow d, \quad (18)$$

where s_d is some subsequence. Then, by the Taylor series expansion, there exists a limiting direction d such that

$$f(z_k) = f(x^*) + (z_k - x^*)^T \nabla f(x^*) + o(\|z_k - x^*\|).$$

Substituting in the limiting direction expression from Equation 18, $(z_k - x^*)^T = \|z_k - x^*\| d^T$:

$$f(z_k) = f(x^*) + \|z_k - x^*\| d^T \nabla f(x^*) + o(\|z_k - x^*\|),$$

and we observe $\|z_k - x^*\| > 0$ and $o(\|z_k - x^*\|) > 0$. Further, $d^T \nabla f(x^*) < 0$, from our assumption.

From the KKT conditions, there exists a local solution $x^* \in \mathcal{O}$ for $k > K \in \mathbb{N}$ such that

$$f(z_k) < f(x^*) + \frac{1}{2} \|z_k - x^*\| \cdot d^T \nabla f(x^*).$$

Since $d^T \nabla f(x^*) \geq 0$ happens when $c_i(x^*) = 0$ and the active set is defined by $\mathcal{A} = \{i \in \mathcal{I} \mid c_i(x^*) = 0\} \cup \mathcal{E}$, the set of tight/active inequality constraints and the equality constraints hold at the optimal solution. Therefore, solving the reduced problem defined by constraints in the active set \mathcal{A} achieves the same solution as solving the full problem. \square

D. Transformer-based Successive Convexification

In this work, we extend T-PDG to the Successive Convexification algorithm, resulting in the Transformer-based Successive Convexification algorithm. We enhance the computational and data efficiency for nonconvex-powered descent guidance by employing symmetry-invariant data augmentation. T-PDG was previously applied to the 3-DoF minimum fuel powered descent guidance problem, improving solution times by up to an order of magnitude compared to LCvx [5]. By learning to predict the set of tight or active constraints at the optimal solution, T-PDG creates the minimal reduced-size problem initialized with only the tight constraints, then uses the solution of this reduced problem to warm-start the direct optimization solver. 6-DoF powered descent guidance is known to be challenging to solve quickly and reliably due to the nonlinear and non-convex nature of the problem, the discretization scheme heavily influencing solution validity, and reference trajectory initialization determining algorithm convergence or divergence. Our contributions in this work address these challenges by extending T-PDG to learn the set of tight constraints for the SCvx formulation of the 6-DoF powered descent guidance problem. In addition to reducing the problem size, feasible and locally optimal reference trajectories are also learned to facilitate convergence from the initial guess. T-PDG enables onboard computation of real-time guidance trajectories, demonstrated by a 6-DoF Mars powered landing application problem.

Algorithm 1 is modified to include an inference step that predicts the set of tight constraints for every convex sub-problem based on the problem parameters and iteration number k . Furthermore, the change in the predicted number of tight constraints is included in the trust region contraction or growth computation to allow the trust region to respond not only to nonlinearity but also to changes in problem structure. The T-SCvx algorithm is presented in Algorithm 2.

Algorithm 2 The T-SCvx Algorithm

- 1: **procedure** T-SCvx($x^1, u^1, \lambda, \epsilon_{\text{tol}}, f_1, f_2$)
- 2: **input:** Predict the solution using the solution prediction Transformer NN $z = f_1(\theta)$ and select initial state with the prediction $(x^1, u^1) = z$. Initialize trust region radius $r^1 > 0$. Select penalty weight $\lambda > 0$, and parameters $0 < \rho_0 < \rho_1 < \rho_2 < 1, r_l > 0$ and $\alpha > 1, \beta > 1$.
- 3: **while** not converged, i.e., $\Delta J^k > \epsilon_{\text{tol}}$ **do**
- 4: **step 1:** At $(k + 1)$ -th succession, predict the set of tight constraints using the trained transformer neural network $\tau = f_2(\theta, k + 1)$. Define the subproblem, Equation 7, using only the constraints identified to be tight.
- 5: **step 2:** Solve Equation 7 at (x^k, u^k, r^k) to get an optimal solution (d, w) .
- 6: **step 3:** Compute the actual change in the penalty cost:

$$\Delta J^k = J(x^k, u^k) - J(x^k + d, u^k + w), \quad (19)$$

where $J(x, u) := C(x, u) + \sum_{i=1}^{N-1} \lambda_i P(x_{i+1} - f(x_i, u_i), s(x_i, u_i))$.

- 7: and the predicted change by the convex cost:

$$\Delta L^k = J(x^k, u^k) - L^k(d, w), \quad (20)$$

where $L^k(d, w) := C(x^k + d, u^k + w) + \sum_{i=1}^{N-1} \lambda_i P(E_i^k v_i, s'_i)$.

- 8: **if** $\Delta J^k = 0$ **then**
- 9: stop, and return (x^k, u^k) ;
- 10: **else**
- 11: compute the ratio

$$\rho^k := \frac{\Delta J^k}{\Delta L^k}. \quad (21)$$

- 12: **end if**
- 13: **step 4:** Compute the percentage of changed constraints $\tau_r = \frac{\sum |\tau_{k+1} - \tau_k|}{\text{len}(\tau_{k+1})}$.
- 14: **step 5:**
- 15: **if** $\rho^k < \rho_0$ **then**
- 16: reject this step, contract the trust region radius, i.e., $r^k \leftarrow \frac{r^k}{\alpha^{\tau_r}}$ and go back to step 1;
- 17: **else**
- 18: accept this step, i.e., $x^{k+1} \leftarrow x^k + d, u^{k+1} \leftarrow u^k + w$, and update the trust region radius r^{k+1} by

$$r^{k+1} = \begin{cases} \frac{r^k}{\alpha^{\tau_r}}, & \text{if } \rho^k < \rho_1; \\ r^k, & \text{if } \rho_1 \leq \rho^k < \rho_2; \\ \beta^{(1-\tau_r)} r^k, & \text{if } \rho_2 \leq \rho^k. \end{cases} \quad (22)$$

- 19: **end if**
 - 20: $r^{k+1} \leftarrow \max\{r^{k+1}, r_l\}, k \leftarrow k + 1$, and go back to step 1.
 - 21: **end while**
 - 22: **return** (x^{k+1}, u^{k+1}) .
 - 23: **end procedure**
-

1. Transformer Neural Network Architecture

The model structure for T-SCvx is considered for the following prediction problem: given a set of parametric inputs for a constrained optimization problem, $\{\theta_1, \dots, \theta_L\}$, we would like to predict the set of tight constraints, $\{\tau(\theta_1), \dots, \tau(\theta_L)\}$, where each $\tau(\theta_i)$ is an $1 \times M$ matrix (M is the number of inequality constraints in the original problem) [5]. Next, linear encoder and decoder layers transfer the input data into a higher dimensional embedding space and the output into a lower dimensional output space. A learned position encoding is then applied to preserve the temporal order of the input data. From the position encoder, a transformer encoder with several heads, h , uses multi-head attention to transform the data into query matrices, $Q_h^{(i)}$, key matrices, $K_h^{(i)}$, and value matrices, $V_h^{(i)}$. Finally, the attention output is generated by scaled production, as shown in Eq. (23).

$$(O_h^{(i)})^T = \text{Attention} \left(Q_h^{(i)}, K_h^{(i)}, V_h^{(i)} \right) = \text{Softmax} \left(\frac{Q_h^{(i)} K_h^{(i)T}}{\sqrt{d_k}} \right) V_h^{(i)} \quad (23)$$

Additional linear layers, dropout, and LayerNorm layers are also present in the transformer encoder layer. The full model was designed in PyTorch using the `torch.nn` module [52]. The implemented tight constraints NN for the 6-DoF PDG application has 1×17 -dimensional problem parameter inputs, including the initial velocity, initial position, angular velocity, initial quaternion, initial mass, pitch angle, glideslope angle, and iteration number, extended from the model trained in [5]. We note that the final position and velocity are set to zero as this application is a powered descent landing problem and, consequently, reference frames can be adjusted accordingly for a varying final position. Additional parameters for the problem can be included and would only result in a larger input size and a potentially larger required neural network architecture. Furthermore, planetary and spacecraft design parameters were kept constant to represent the chosen mission design. Since state and constraint parameters may change during operation, these variables were chosen as the parameters for the parametric optimization problem.

E. T-SCvx Algorithm

Algorithm 3 describes the procedure for applying the transformer NNs for problem reduction in real-time. First, the NN models for predicting tight constraints are called to generate the strategy at iteration $k + 1$. Using the strategy, the solver is called to find the corresponding solution and cost, as determined by the problem's cost function. Since the full problem is used for the evaluation cost function, T-SCvx will not return a solution unless it is both optimal and constraint satisfying for the full problem.

Algorithm 3 T-SCvx

- 1: **procedure** T-SCvx($\theta, k+1$)
 - 2: $strategy \leftarrow \text{NN-PREDICTION}(\text{tight_constraints_model}, \theta, k + 1)$ ▷ Predict the optimal strategy
 - 3: $(soln, cost) \leftarrow \text{REDUCED-SOLVE}(\theta, strategy)$
 - 4: **return** $soln$
 - 5: **end procedure**
-

To acquire the samples required for training, we use the SCvx algorithm from the SCP Toolbox, which uses the ECOS solver [53]* [21]. A custom implementation of the free final time 6-DoF minimum fuel powered descent guidance problem presented in Equations (2)-(6) was programmed in Julia. Utilizing the solver, we efficiently sample feasible regions of the solution space to accelerate the convergence of the optimization process. Numerical scaling was used for variable ranges to ensure the solver was well-conditioned. Because the 6-DoF powered descent guidance problem is non-convex, advanced sampling methods must be used to avoid computational inefficiencies by avoiding non-feasible regions in the solution space.

1. Symbolic Implementation of the 6-DoF Problem

To utilize SCvx to iteratively solve the non-convex optimization problem, the problem must be linearized and discretized. The dynamics, kinematics, and constraints are linearized through the Jacobian matrix. The state vector $\mathbf{x}(t)$ and control vector $\mathbf{u}(t)$ are defined as follows:

$$\mathbf{x}(t) = [\mathbf{r}(t) \quad \mathbf{v}(t) \quad \mathbf{q}(t) \quad \boldsymbol{\omega}(t) \quad m(t)]^T \quad (24)$$

$$\mathbf{u}(t) = \mathbf{T}(t) \quad (25)$$

The Jacobian matrix of the convex constraints defined in Equation 4 with respect to the state vector and control vector is defined as:

$$\mathbf{A}(t) = \frac{\partial \mathbf{f}}{\partial \mathbf{x}}, \quad \mathbf{B}(t) = \frac{\partial \mathbf{f}}{\partial \mathbf{u}} \quad (26)$$

The partial derivatives required to calculate the matrix in 6-DoF rely on quaternion and skew-symmetric matrix derivative calculations and thus require symbolic differentiation to derive the matrix analytically. Our method uses

*<https://github.com/jump-dev/ECOS.jl>

Symbolics package in Julia to define the partial derivatives efficiently and avoid numerical errors in finite difference methods. The partial derivatives are calculated at each time step and assembled into the Jacobian matrices $\mathbf{A}(t)$ and $\mathbf{B}(t)$. The process is repeated at each time step in the successive convexification process as laid out in Equation (7).

2. Data Sampling Strategy

Since the 6-DoF powered descent guidance problem is non-convex, using a naive uniform sampling algorithm like T-PDG in 3-DoF uses would be too computationally inefficient to generate a sizable dataset for training. Therefore, our sampling strategy utilizes the symmetry of the system dynamics and constraint activation to efficiently sample over a wide range of initial conditions. Every initial sample was sampled with only a positive range of East and North initial condition coordinates. Next, a rotation about the Up axis was computed at the angles 0° , 45° , 90° , 135° , 180° , 225° , 270° , and 315° . We note that all induced constraints are symmetric about the Up axis, so the set of tight constraints that are mapped to remain invariant under these rotations. By synthetically rotating the dataset around the up axis, sampling efficiency is achieved while encoding symmetries into the NN. In this work, we sampled a dataset of tight constraints and optimal solutions consisting of less than 1,600 samples. After performing the set of rotations the dataset reached over 11,600 samples. Further, this method of data augmentation has been shown to have similar accuracies to rotational invariant NN architectures [54].

3. Training, Validation, and Testing

The transformer NN architecture (described in Section III.D.1) implemented for T-PDG was utilized for both the tight constraints prediction and solution prediction NNs in T-SCvx. All sampled data, including the rotated samples, were split into 80% training and validation data and 20% test data. The datasets were standardized by subtracting the mean and dividing by the standard deviation and a K-fold training process was utilized with $K = 3$, 4000 warmup steps, and two epochs. MSE loss was used for training and testing the solution neural network, while binary loss was used for testing the tight constraint prediction neural network. Applying T-PDG to 6-DoF powered descent guidance improves the initial guess for SCP algorithms and can indicate the predicted number of active constraints. Furthermore, T-SCvx efficiently determines if superlinear convergence holds for the problem (see Section III.B.1).

IV. Transformer-based Successive Convexification

A. Problem Setup and Parameters

The problem parameters are shown in Table 1, where the units are dimensionless quantities of length U_L , time U_T , and mass U_M to improve numerical scaling for the solver. The same problem parameters were used for successive convexification, except for the trust region initialization, η_{init} , where a smaller trust region was used for T-SCvx since we assume we are already very close to the final solution when an initial guess is predicted, in addition to ensuring trust region conservatism in the case the guess or tight constraints were not fully accurate. A total of 1,592 samples were computed using the SCvx algorithm (Algorithm 1), and rotations were then computed on the data, as described in Section III.E.2, to create a dataset of 11,634 samples. Throughout this study, SCvx was limited to 20 iterations maximum. If the algorithm does not converge when the maximum iteration number is met, the problem is considered infeasible. The parameters sampled over include $\theta = \gamma_{gs}, \theta_{\max}, r_0, v_0, q_0, \omega_0, m_0$, including the glideslope angle, maximum pitch angle, initial position, initial velocity, initial quaternion, initial angular velocity, and initial mass. Representing the full initial state for 6-DoF motion and constraint parameters which may vary between the parachute and powered descent initiation phase. An additional extension from 3-DoF T-PDG includes the addition of the mass parameter, allowing multiple trajectories to be computed during the descent process instead of assuming only one trajectory is generated at powered descent initiation. For the tight constraint prediction NN, an additional parameter of the SCvx iteration number, k , is included so the NN can predict the tight constraints for a given iteration number. The final state is maintained constant since a change in the reference frame can be used to represent any desired configuration. The strategy is a binary vector $\tau(\theta)$ corresponding to the inequality constraints (5-6). We note that the implementation of T-SCvx (Algorithm 2) only uses the convex constraints to reduce the convex subproblems, but an extension could be easily made to reduce the non-convex cost function based on the predicted non-convex tight constraints. Instead of only a final time prediction neural network, T-SCvx maps to the full discretized solution, including the full state, control, and final time parameter (x, u, t_f) , and this enables an accurate initial guess to be generated.

The NNs for tight constraint and solution prediction used the transformer architecture in Section III.D.1. The

Table 1 Problem Parameters

Param.	Value	Units
g_I	$-\mathbf{e}_1$	U_L/U_T^2
ρ	0.020	U_M/U_L^3
\mathbf{J}_B	0.01 $\text{diag}[0.1 \ 1 \ 1]$	$U_M \cdot U_L^2$
P_{amb}	0.1	$U_M/U_T^2/U_L$
A_{noz}	0.5	U_L^2
$r_{\text{cp},B}$	$0_{3 \times 1}$	U_L
$r_{T,B}$	$-0.01 \cdot e_1$	U_L
$\rho S_A C_A$	0.2	-
I_{sp}	30.0	U_T
ω_{max}	90.0	$^\circ/U_T$
δ_{max}	20.0	$^\circ$
T_{min}	0.3	$U_M \cdot U_L/U_T^2$
T_{max}	5.0	$U_M \cdot U_L/U_T^2$
V_α	2.0	U_L/U_T
m_{dry}	2.0	U_M
$\mathbf{r}_{I,N}$	$0_{3 \times 1}$	U_L
$\mathbf{v}_{I,N}$	$-0.1 \cdot e_1$	U_L/U_T
$\omega_{\mathcal{B},1}, \omega_{\mathcal{B},N}$	$0_{3 \times 1}$	$^\circ/U_T$
$\mathbf{q}_{B \leftarrow I,N}$	q_{id}	-
N	50	-
N_{sub}	49	-
iter_{max}	20	-
disc method	FOH	-
λ	500	-
ρ_0	0	-
ρ_1	0.1	-
ρ_2	0.7	-
β_{sh}	2.0	-
β_{gr}	2.0	-
$\eta_{\text{full, init}}$	2.0	-
$\eta_{\text{reduced, init}}$	0.01	-
η_{lb}	0.001	-
η_{ub}	10.0	-
ϵ_{abs}	0.1	-
ϵ_{rel}	0.001	-
feas tol	0.5	-
q_{tr}	Inf	-
q_{exit}	Inf	-
solver	ECOS	-
solver maxit	1000	-

constraint prediction NN has an input size of 17 and an output size of 12N, using an architecture with 384-dimensional layers, two heads, four layers, and 0.1 dropout. The solution prediction NN, was designed to be larger since the input size of 16 corresponded to an output size of 17N+1. 768-dimensional layers were used, with two heads, four layers, and 0.1 dropout. The range of values sampled for NN training is included in Table 2.

B. Results and Analysis

Utilizing the training process described in Section III.E.3, the tight constraint prediction and solution NNs were trained with less than 12,000 samples, most of which were produced using efficient rotation-based data augmentation. Both NNs converged within two epochs of training for batch sizes of 128. Table 3 shows the training and validation MSE

Table 2 Sampled Dataset

Parameter	Min Range	Max Range
K	1	20
Glideslope angle (γ_{gs})	0 deg	90 deg
Pitch angle (θ_{\max})	0 deg	359.4 deg
Initial Position (r_0)	0.003 \hat{e}_x+	9.997 \hat{e}_x+
	-13.83 \hat{e}_y+	13.83 \hat{e}_y+
	-13.83 \hat{e}_z	13.83 \hat{e}_z
Initial Velocity (v_0)	-1.998 \hat{e}_x+	-0.001 \hat{e}_x+
	-2.779 \hat{e}_y+	2.779 \hat{e}_y+
	-2.779 \hat{e}_z	2.779 \hat{e}_z
Initial Quaternion (q_0)	-0.996 + -1 $i+$	1 + 1 $i+$ 1 $j+$
	-1 $j+$ -1 k	0.999 k
Initial Angular Velocity (ω_0)	-89.98 \hat{e}_x+	89.70 \hat{e}_x+
	-123.49 \hat{e}_y+	123.49 \hat{e}_y+
	-123.49 \hat{e}_z deg	123.49 \hat{e}_z deg
Initial mass (m_0)	0.003	3

at the third fold of training and the accuracy of each NN on the test dataset. Since the predicted constraints are binary, binary accuracy was used for test time evaluation, while MSE was used for the floating point solution prediction values.

Table 3 Training and Testing of T-SCvx with Baseline Comparisons

Model	Train (MSE)	Validation (MSE)	Test (MSE / Binary Acc.)	# of Params
Constraint NN	0.024	0.024	96.45% (Binary Acc.)	8.91M
Solution NN	0.975	1.092	1.040 (MSE)	9M
Predict Only Zeros	-	-	95.95% (Binary Acc.)	-
Predict Only Ones	-	-	4.05% (Binary Acc.)	-

The results from T-SCvx, from Algorithm 2, compared to SCvx, using 545 samples from the test dataset, are shown in Figure 2. From the test results, T-SCvx reduces the mean solve time for the 50-timestep 6-DoF powered descent guidance problem by 66% and the median solve time by 70%. The standard deviation for T-SCvx is slightly higher than SCvx, at 5.24 seconds, but one standard deviation remains below the SCvx mean of 14.61.

Figure 3 shows three T-SCvx-computed test trajectories. Multiple orientations, initial positions, and velocities are resolved by the solver, computing the control strategy required to reach the final position. Compared to T-PDG, T-SCvx extends the predictive capabilities to include not only convex tight constraints at every convex subproblem iteration but also the full state, control, and final time solution initial guess. Returned solution feasibility is ensured by keeping the full problem penalty cost and not converging until the actual change in the penalty cost is zero. A new addition to the trust region radius augments the contraction and growth parameters to scale by changing the number of tight constraints from the last iteration. This update enables a reduced trust region radius when a large change in the predicted tight constraints occurs. With the addition of tight constraint prediction and full solution prediction using transformer NNs, the mean solve time of almost 15 seconds for SCvx was reduced to less than 5 seconds for T-SCvx when applied to the Mars 6-DoF PDG problem for free final time. Given this significant decrease, T-SCvx serves as a potential candidate for high-fidelity large divert guidance trajectory generation.

C. Benchmarking with Table Lookup Approaches

In this section we demonstrate the trade-offs between lookup table methods and using T-SCvx. Lookup tables serve as a potential alternative to learning-based methods. Previous work in powered descent guidance has explored linear interpolation-based lookup tables for solution and final time prediction [55, 56]. Of particular note is that these linear interpolation-based methods assume close to convex or highly discretized problems, to ensure nonlinearities in solution do not result in high prediction errors. This section explores the effects of table lookup approaches on the non-convex 6-DoF powered descent guidance dataset.

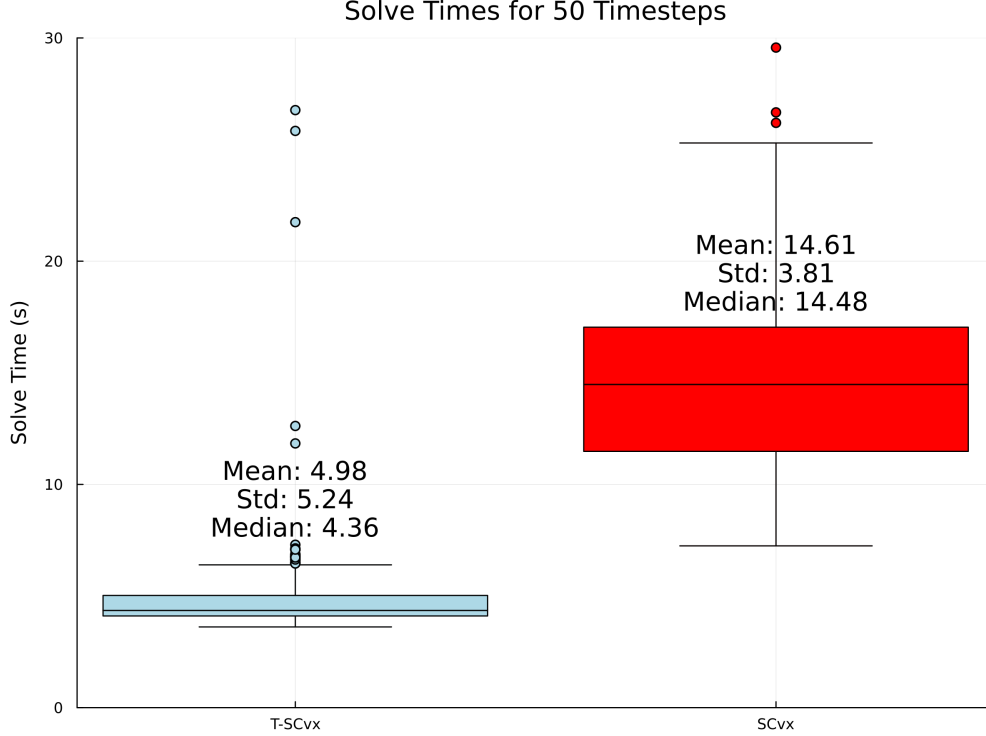


Fig. 2 Box plots for T-SCvx and SCvx showing mean, median, and standard deviations.

Further, a KD-tree for nearest neighbor lookups approach was compared in this work [57]. For ease of comparison, the table lookup methods use the same training and test data and predict the same quantities as T-SCvx. Due to the high inference time and memory requirements of the linear interpolation method, the training and test data were both reduced to 10 components using principal component analysis (PCA), implemented with `sklearn.decomposition`, and then a subset of 100 samples was used for training and 10 samples for testing [58, 59].

Tables 4 and 5 show the inference time, mean-squared-errors (MSE), out-of-distribution (OOD) MSEs, and peak memory usage for the KDTree and T-SCvx. Where OOD test data was categorized using the 95th percentile for the Mahalanobis distance: $d_M(\mathbf{x}, Q) = \sqrt{(\mathbf{x} - \mu)^T S^{-1} (\mathbf{x} - \mu)}$, where $Q \in \mathbb{R}^N$ is the training dataset’s probability distribution with mean μ and covariance S and \mathbf{x} is the test data point [60]. Figure 4 shows each algorithm type’s memory usage and inference time means and standard deviations. Results are compared against a one-second runtime requirement and 60 MB of Static Random Access Memory (SRAM)* for a RAD750 flight computer [61].

Table 4 Tight Constraints Prediction Performance

Metric	Linear Interpolation	KDTree	T-SCvx
Inference Time (ms)	894.02	0.1500	4.5929
MSE	0.0368	0.0074	0.0241
OOD MSE	0.0700	0.0657	0.0373
Peak Memory Usage (MB)	1647.0	3.300	2.634

From Table 4, T-SCvx reduces inference time, when compared to linear interpolation, by over 99% and memory usage by 99.8% for tight constraints prediction. Further, the T-SCvx has a comparatively lower MSE, when compared to linear interpolation. Impressively, the kd-tree nearest neighbors approach dominates all algorithms for inference time and accuracy, with sub-millisecond inference times and 0.0074 MSE. This high accuracy does not carry over to OOD data though, as T-SCvx dominates all methods for OOD accuracy. A similar pattern is observed for Table 5, where T-SCvx dominates the linear interpolation approach for solution prediction, reducing inference time and peak

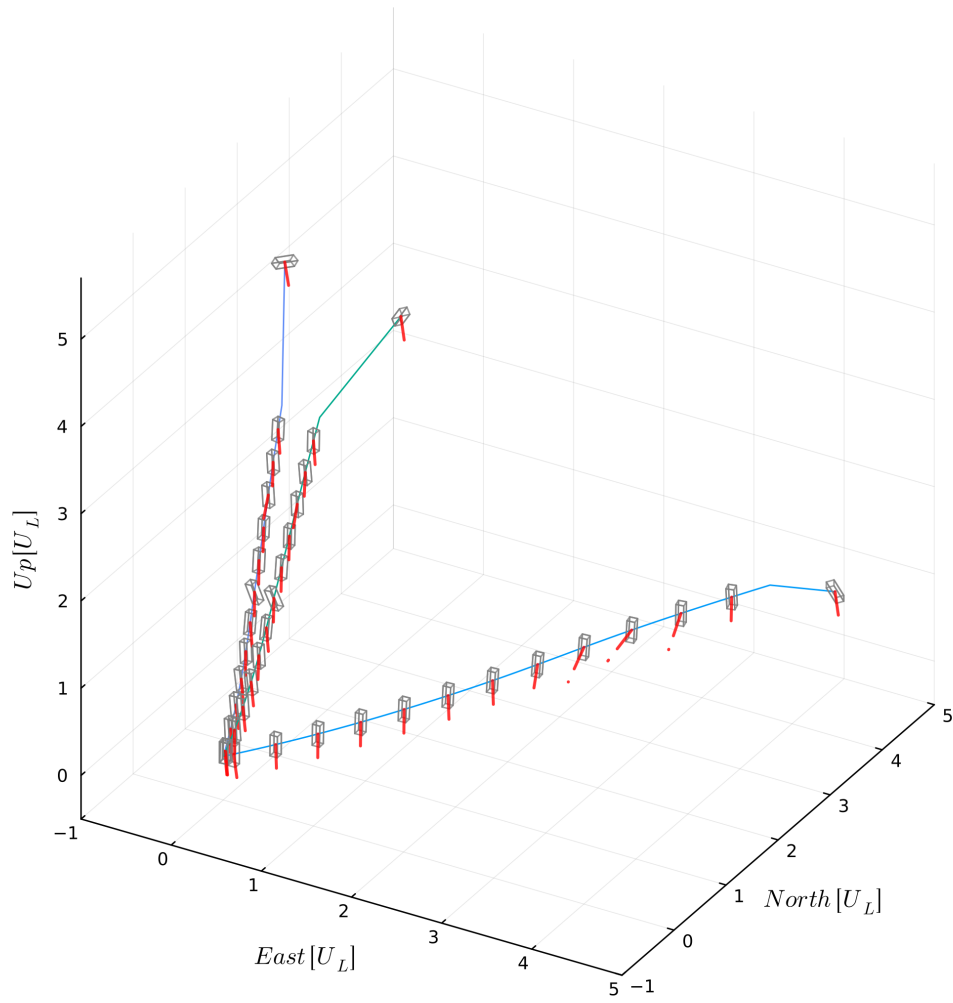


Fig. 3 6-DoF minimum fuel trajectory computed by T-SCvx with thrust vectors in red.

Table 5 Solution Prediction Performance

Metric	Linear Interpolation	KDTree	T-SCvx
Inference Time (ms)	904.43	0.1411	4.9492
MSE	0.8176	0.6326	1.0450
OOD MSE	2.3195	2.4128	1.1093
Peak Memory Usage (MB)	1678.5	1.5987	9.0118

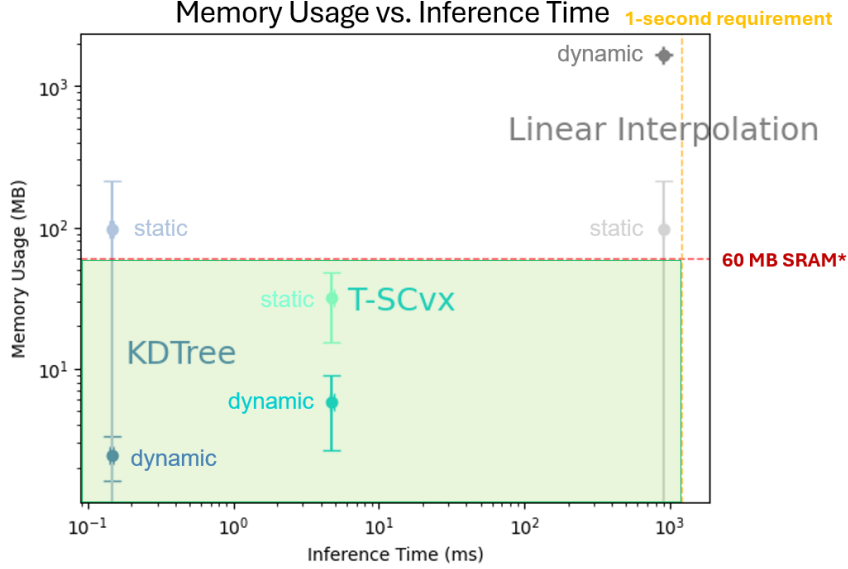


Fig. 4 Memory vs. inference time for each warm-start algorithm type.

memory usage by 99.5%. Interestingly, the linear interpolation and kd-tree lookup approaches have slightly higher accuracies, while still not maintaining the low accuracies for OOD data. The novel kd-tree approach is particularly performant for the solution prediction problem, dominating inference time accuracy, and peak memory usage. It must be noted that the MSE more than doubles when OOD samples are used for the kd-tree, as opposed to T-SCvx, which has a mostly consistent MSE when faced with OOD data. Overall, the kd-tree has been demonstrated to perform well for the 6-DoF tight constraint prediction and solution prediction problems, but this performance does not extend to out-of-distribution samples. Compared to the state-of-the-art linear interpolation-based lookup table in powered descent guidance literature, T-SCvx exhibits superior performance in inference time, tight constraint prediction accuracy, and memory usage.

V. Future Work

While the results obtained for T-SCvx are promising for improving the computational efficiency and interpretability of the powered descent guidance problem, several future directions can be explored. As discussed previously, knowledge of or an estimate of the set of tight constraints not only serves as a high-quality warm-start for a numerical optimization problem, but it can also provide insight into the type of convergence guarantees provided by the solver. As the trust region formulation largely determines iteration number and convergence for the SCvx algorithm, additional informed developments of trust region designs could be done using transformer-generated predictions. Further, a promising area of research would be to dovetail our tight constraint prediction framework into an existing active set-based nonlinear program solver [28], potentially further increasing computational efficiency. Finally, sparsity in linear algebra operations is advantageous for efficient linear algebra operations and future use of tight constraint predictions could inform custom solve implementations to promote sparsity in matrix operations [62].

The next steps for this work include verifying the solve time gains are representative of flight-grade radiation-hardened hardware. Novel contributions include programming, verifying, and validating the use of trained deep neural networks

on hardware. This includes testing T-PDG and T-SCvx with custom solver implementations and developing efficient parallel algorithmic updates where possible.

VI. Conclusion

We have demonstrated the contribution of Transformer-based Successive Convexification for 6-DoF powered descent guidance, including a 6-DoF Mars powered descent guidance test problem. The main contributions of T-SCvx include enhanced computational efficiency and reliability in solve times for non-convex trajectory generation, enabled by the design of transformer NNs for tight constraint and solution initial guess prediction. By mapping the initial state and constraint parameters to the tight constraints and problem state, control, and final time with a transformer NN, a variety of initial conditions and problem parameters are accounted for. Additionally, the introduction of a rotation-invariant data augmentation method reduced the number of required samples to under 2,000 to achieve test accuracies of over 96% and under 1 MSE. As expected, for the 6-DoF powered descent guidance problem, Transformer-based Powered Descent Guidance demonstrated a greater reduction in mean runtime, with T-SCvx reducing the mean runtime by 66%; runtime was reduced by 9.63 seconds when compared to SCvx. Benchmarking against linear interpolation approaches suggested in the literature showed T-SCvx to reduce the required inference time and memory usage by more than 99%, with greater or comparable accuracy. The kd-tree nearest neighbor approach serves as a more interpretable alternative, applicable when test data is not out-of-distribution.

Further, the convergence criteria remained the same as SCvx, requiring returned trajectories to satisfy all problem constraints and maintain the feasibility of returned solutions. An additional update from T-PDG includes the initial mass as a parameter in T-SCvx, allowing for trajectories to be computed even after powered descent initiation. T-SCvx has been successfully demonstrated as a potential trajectory optimization for fast high-fidelity guidance scenarios, including the application problem of 6-DoF Mars landing.

Acknowledgments

This work was supported in part by a NASA Space Technology Graduate Research Opportunity 80NSSC21K1301. This research was carried out in part at the Jet Propulsion Laboratory, California Institute of Technology, under a contract with the National Aeronautics and Space Administration and funded through the internal Research and Technology Development program.

References

- [1] Shuster, M. D., "A survey of attitude representations," *Journal of the Astronautical Sciences*, Vol. 41, No. 4, 1993, pp. 439 – 517.
- [2] Szmuk, M., Reynolds, T. P., and Açıkmeşe, B., "Successive Convexification for Real-Time Six-Degree-of-Freedom Powered Descent Guidance with State-Triggered Constraints," *AIAA Journal of Guidance, Control, and Dynamics*, Vol. 43, No. 8, 2020, pp. 1399–1413.
- [3] Izzo, D., Märten, M., and Pan, B., "A survey on artificial intelligence trends in spacecraft guidance dynamics and control," *Astrodynamics*, Vol. 3, 2019, pp. 287–299.
- [4] Guffanti, T., Gammelli, D., D'Amico, S., and Pavone, M., "Transformers for Trajectory Optimization with Application to Spacecraft Rendezvous," *IEEE Aerospace Conference*, 2024.
- [5] Briden, J., Gurga, T., Johnson, B. J., Cauligi, A., and Linares, R., "Improving Computational Efficiency for Powered Descent Guidance via Transformer-based Tight Constraint Prediction," *AIAA Scitech Forum*, 2024.
- [6] Lu, P., Forbes, S., and Baldwin, M., "A Versatile Powered Guidance Algorithm," *AIAA Conf. on Guidance, Navigation and Control*, 2012.
- [7] Lu, P., "Propellant-Optimal Powered Descent Guidance," *AIAA Journal of Guidance, Control, and Dynamics*, Vol. 41, No. 4, 2018, pp. 813–826.
- [8] Kirk, D. E., *Optimal control theory: an introduction*, Courier Corporation, 2012.
- [9] Klumpp, A. R., "Apollo Lunar Descent Guidance," *Automatica*, Vol. 10, No. 2, 1974, pp. 133–146.

- [10] Najson, F., and Mease, K. D., “Computationally Inexpensive Guidance Algorithm for Fuel-Efficient Terminal Descent,” *AIAA Journal of Guidance, Control, and Dynamics*, Vol. 29, No. 4, 2006, pp. 955–964.
- [11] Topcu, U., Casoliva, J., and Mease, K. D., “Minimum-Fuel Powered Descent for Mars Pinpoint Landing,” *AIAA Journal of Spacecraft and Rockets*, Vol. 44, No. 2, 2007, pp. 324–331.
- [12] Sostaric, R. R., and Rea, J. R., “Powered descent guidance methods for the Moon and Mars,” *AIAA Conf. on Guidance, Navigation and Control*, 2005.
- [13] Byrd, R. H., Gould, N. I. M., Nocedal, J., and Waltz, R. A., “An Algorithm for Nonlinear Optimization Using Linear Programming and Equality Constrained Subproblems,” *Mathematical Programming*, Vol. 100, 2003, pp. 27–48.
- [14] Palacios-Gomez, F., Lasdon, L., and Engquist, M., “Nonlinear Optimization by Successive Linear Programming,” *Management Science*, Vol. 28, No. 10, 1982, pp. 1106–1120.
- [15] Horst, R., and Thoai, N. V., “DC programming: Overview,” *Journal of Optimization Theory & Applications*, Vol. 103, 1999, pp. 1–43.
- [16] Yuille, A., and Rangarajan, A., “The Concave-Convex Procedure (CCCP),” *Conf. on Neural Information Processing Systems*, 2001.
- [17] Liu, X., and Lu, P., “Solving Nonconvex Optimal Control Problems by Convex Optimization,” *AIAA Journal of Guidance, Control, and Dynamics*, Vol. 37, No. 3, 2014, pp. 750 – 765.
- [18] Liu, X., Shen, Z., and Lu, P., “Entry trajectory optimization by second-order cone programming,” *AIAA Journal of Guidance, Control, and Dynamics*, Vol. 39, No. 2, 2015, pp. 227–241.
- [19] Mao, Y., Szmuk, M., and Açıkmeşe, B., “Successive Convexification of Non-Convex Optimal Control Problems and Its Convergence Properties,” *Proc. IEEE Conf. on Decision and Control*, 2016.
- [20] Wang, Z., and Grant, M. J., “Constrained Trajectory Optimization for Planetary Entry via Sequential Convex Programming,” *AIAA Journal of Guidance, Control, and Dynamics*, Vol. 40, No. 10, 2017, pp. 2603 – 2615.
- [21] Malyuta, D., Reynolds, T. P., Szmuk, M., Lew, T., Bonalli, R., Pavone, M., and Açıkmeşe, B., “Convex Optimization for Trajectory Generation: A Tutorial on Generating Dynamically Feasible Trajectories Reliably and Efficiently,” *IEEE Control Systems Letters*, Vol. 42, No. 5, 2022, pp. 40–113.
- [22] Han, S. P., “A Globally Convergent Method for Nonlinear Programming,” *Journal of Optimization Theory & Applications*, Vol. 22, No. 3, 1977, pp. 297–309.
- [23] Powell, M. J., “Algorithms for Nonlinear Constraints that use Lagrangian Functions,” *Mathematical Programming*, Vol. 14, No. 1, 1978, pp. 224–248.
- [24] Powell, M. J., and Yuan, Y., “A Recursive Quadratic Programming Algorithm that uses Differentiable Exact Penalty Functions,” *Mathematical Programming*, Vol. 35, 1986, pp. 265–278.
- [25] Boggs, P. T., and Tolle, W. J., “A Strategy for Global Convergence in a Sequential Quadratic Programming Algorithm,” *SIAM Journal on Numerical Analysis*, Vol. 26, No. 3, 1989, pp. 600–623.
- [26] Boggs, P. T., and Tolle, W. J., “Sequential Quadratic Programming,” *Acta Numerica*, Vol. 4, 1995, pp. 1–52.
- [27] Fukushima, M., “A Successive Quadratic Programming Algorithm with Global and Superlinear Convergence Properties,” *Mathematical Programming*, Vol. 35, 1986, pp. 253–264.
- [28] Gill, P. E., Murray, W., and Saunders, M. A., “SNOPT: An SQP algorithm for large-scale constrained optimization,” *SIAM Review*, Vol. 47, No. 1, 2005, pp. 99–131.
- [29] Betts, J. T., and Huffman, W. P., “Path-Constrained Trajectory Optimization using Sparse Sequential Quadratic Programming,” *AIAA Journal of Guidance, Control, and Dynamics*, Vol. 16, No. 1, 1993, pp. 59–68.
- [30] Açıkmeşe, B., and Blackmore, L., “Lossless Convexification of a Class of Optimal Control Problems with Non-Convex Control Constraints,” *Automatica*, Vol. 47, No. 2, 2011, pp. 341–347.
- [31] Harris, M., and Açıkmeşe, B., “Lossless Convexification of Non-convex Optimal Control Problems for State Constrained Linear Systems,” *Automatica*, Vol. 50, No. 9, 2014, pp. 2304–2311.

- [32] Blackmore, L., Açıkmeşe, B., and Carson, J. M., “Lossless convexification of control constraints for a class of nonlinear optimal control problems,” *Systems & Control Letters*, Vol. 61, No. 4, 2012, pp. 863–871.
- [33] Açıkmeşe, B., and Ploen, S. R., “A powered descent guidance algorithm for Mars pinpoint landing,” *AIAA Conf. on Guidance, Navigation and Control*, 2005.
- [34] Açıkmeşe, B., and Ploen, S. R., “Convex Programming Approach to Powered Descent Guidance for Mars Landing,” *AIAA Journal of Guidance, Control, and Dynamics*, Vol. 30, No. 5, 2007, pp. 1353–1366.
- [35] Blackmore, L., Açıkmeşe, B., and Scharf, D. P., “Minimum Landing Error Powered Descent Guidance for Mars Landing using Convex Optimization,” *AIAA Journal of Guidance, Control, and Dynamics*, Vol. 33, No. 4, 2010.
- [36] Açıkmeşe, B., Carson, J., and Blackmore, L., “Lossless Convexification of Non-convex Control Bound and Pointing Constraints of the Soft Landing Optimal Control Problem,” *IEEE Transactions on Control Systems Technology*, Vol. 21, No. 6, 2013, pp. 2104–2113.
- [37] Harris, M. W., and Açıkmeşe, B., “Maximum Divert for Planetary Landing Using Convex Optimization,” *Journal of Optimization Theory & Applications*, 2013, pp. 1–21.
- [38] Dueri, D., Zhang, J., and Açıkmeşe, B., “Automated Custom Code Generation for Embedded, Real-time Second Order Cone Programming,” *IFAC World Congress*, 2014.
- [39] Dueri, D., Açıkmeşe, B., Scharf, D. P., and Harris, M. W., “Customized Real-Time Interior-Point Methods for Onboard Powered-Descent Guidance,” *AIAA Journal of Guidance, Control, and Dynamics*, Vol. 40, No. 2, 2017, pp. 197–212.
- [40] Boyd, S., and Vandenberghe, L., *Convex Optimization*, Cambridge Univ. Press, 2004.
- [41] Nocedal, J., and Wright, S. J., *Numerical Optimization*, 2nd ed., Springer, 2006.
- [42] Lee, U., and Mesbahi, M., “Optimal Power Descent Guidance with 6-DoF Line of Sight Constraints via Unit Dual Quaternions,” *AIAA Scitech Forum*, 2015.
- [43] Lee, U., and Mesbahi, M., “Constrained Autonomous Precision Landing via Dual Quaternions and Model Predictive Control,” *AIAA Journal of Guidance, Control, and Dynamics*, 2016.
- [44] Cauligi, A., Culbertson, P., Stellato, B., Bertsimas, D., Schwager, M., and Pavone, M., “Learning Mixed-Integer Convex Optimization Strategies for Robot Planning and Control,” *Proc. IEEE Conf. on Decision and Control*, 2020.
- [45] Cauligi, A., Culbertson, P., Schmerling, E., Schwager, M., Stellato, B., and Pavone, M., “CoCo: Online Mixed-Integer Control via Supervised Learning,” *IEEE Robotics and Automation Letters*, Vol. 7, No. 2, 2022, pp. 1447–1454.
- [46] Cauligi, A., Chakrabarty, A., Di Cairano, S., and Quirynen, R., “PRISM: Recurrent neural networks and presolve methods for fast mixed-integer optimal control,” *Learning for Dynamics & Control*, 2022.
- [47] Szmuk, M., and Açıkmeşe, B., “Successive Convexification for 6-DoF Mars Rocket Powered Landing with Free-Final-Time,” *AIAA Scitech Forum*, 2018.
- [48] Bernardini, N., Baresi, N., and Armellin, R., “State-Dependent Trust Region for Successive Convex Programming for Autonomous Spacecraft,” *Astrodynamics*, Vol. 8, 2024, pp. 553–575.
- [49] Attouch, H., Bolte, J., and Svaiter, B. F., “Convergence of Descent Methods for Semi-Algebraic and Tame Problems: Proximal Algorithms, Forward–Backward Splitting, and Regularized Gauss–Seidel Methods,” *Mathematical Programming*, Vol. 137, No. 1-2, 2013, pp. 91–129.
- [50] Elango, P., Luo, D., Kamath, A. G., Uzun, S., Kim, T., and Açıkmeşe, B., “Successive Convexification for Trajectory Optimization with Continuous-Time Constraint Satisfaction,” *ArXiv Preprint*, 2024. Available at <https://arxiv.org/abs/2404.16826>.
- [51] Calafiore, G. C., “Random Convex Programs,” *SIAM Journal on Optimization*, Vol. 20, No. 6, 2010.
- [52] Paszke, A., Gross, S., Chintala, S., Chanan, G., Yang, E., DeVito, Z., Lin, Z., Desmaison, A., Antiga, L., and Lerer, A., “Automatic differentiation in PyTorch,” *Conf. on Neural Information Processing Systems - Autodiff Workshop*, 2017.
- [53] Domahidi, A., Chu, E., and Boyd, S., “ECOS: An SOCP solver for embedded systems,” *European Control Conference*, 2013.
- [54] Quiroga, F., Ronchetti, F., Lanzarini, L., and Bariviera, A. F., “Revisiting Data Augmentation for Rotational Invariance in Convolutional Neural Networks,” *Int. Conf. on Modelling and Simulation in Management Sciences*, 2019.

- [55] Açıkmeşe, B., Blackmore, L., Scharf, D. P., and Wolf, A., “Enhancements on the Convex Programming Based Powered Descent Guidance Algorithm for Mars Landing,” *AIAA/AAS Astrodynamics Specialist Conference*, 2008.
- [56] Scharf, D. P., Ploen, S. R., and Açıkmeşe, B., “Interpolation-Enhanced Powered Descent Guidance for Onboard Nominal, Off-Nominal, and Multi-X Scenarios,” *AIAA Conf. on Guidance, Navigation and Control*, 2015.
- [57] Bentley, J. L., “Multidimensional binary search trees used for associative searching,” *Communications of the ACM*, Vol. 18, No. 9, 1975, pp. 509–517.
- [58] Pearson, K., “On Lines and Planes of Closest Fit to Systems of Points in Space,” *Philosophical Magazine*, Vol. 2, No. 11, 1901, pp. 559–572.
- [59] Pedregosa, F., Varoquaux, G., Gramfort, A., Michel, V., Thirion, B., Grisel, O., Blondel, M., Prettenhofer, P., Weiss, R., Dubourg, V., Vanderplas, J., Passos, A., Cournapeau, D., Brucher, M., Perrot, M., and Duchesnay, E., “Scikit-learn: Machine Learning in Python,” *Journal of Machine Learning Research*, Vol. 12, 2011, pp. 2825–2830.
- [60] De Maesschalck, R., Jouan-Rimbaud, D., and Massart, D. L., “The Mahalanobis distance,” *Chemometrics and Intelligent Laboratory Systems*, Vol. 50, No. 1, 2000, pp. 1–18.
- [61] Berger, R., Dennis, A., Eckhardt, D., Miller, S., Robertson, J., Saridakis, D., Stanley, D., Vancampen, M., and Nguyen, Q., “RAD750™ SpaceWire-Enabled Flight Computer for Lunar Reconnaissance Orbiter,” *International SpaceWire Conference*, 2007.
- [62] Booker, M., and Majumdar, A., “Learning to Actively Reduce Memory Requirements for Robot Control Tasks,” *Learning for Dynamics & Control*, 2021.